

A numerical method to estimate uncertainty in non-rigid structure from motion

Jingwei Song, Mitesh Patel, *Member, IEEE*

Abstract—Semi-Definite Programming (SDP) with low-rank prior has been widely applied in Non-Rigid Structure from Motion (NRSfM). Based on a low-rank constraint, it avoids the inherent ambiguity of basis number selection in conventional base-shape or base-trajectory methods. Despite the efficiency in deformable shape reconstruction, it remains unclear how to assess the uncertainty of the recovered shape from the SDP process. In this paper, we present a statistical inference on the element-wise uncertainty quantification of the estimated deforming 3D shape points in the case of the exact low-rank SDP problem. A closed-form uncertainty quantification method is proposed and tested. Moreover, we extend the exact low-rank uncertainty quantification to the approximate low-rank scenario with a numerical optimal rank selection method, which enables solving practical application in SDP based NRSfM scenario. The proposed method provides an independent module to the SDP method and only requires the statistic information of the input 2D tracked points. Extensive experiments prove that the output 3D points have identical normal distribution to the 2D trackings, the proposed method and quantify the uncertainty accurately, and supports that it has desirable effects on routinely SDP low-rank based NRSfM solver.

I. INTRODUCTION

Non-Rigid Structure from Motion (NRSfM) is the topic of recovering the camera motion and the 3D time-varying shape of a/the deformable object/objects simultaneously from monocular images with sequential 2D trajectories. It contributes to the 3D shape perception with various applications like 3D reconstruction and scene understanding, using consumer-level digital cameras. Thus, NRSfM is widely applied in the field of recovering human pose, face or surgical organs with the stream of monocular video. However, observing a partial 2D projection, the NRSfM method faces heavy ambiguity which poses great difficulty for accurate 3D reconstruction. To overcome the under-constrained issue, different priors are proposed to enable shape estimation in sacrifice for small motion details. These methods can be classified as geometry-based and machine learning-based. Moreover, the geometry-based methods can be categorized into two subclasses: factorization with predefined bases and nuclear norm minimization approaches.

Despite the progress in NRSfM, no research pays attention to the quantify confidence of the reconstructed shape in NRSfM. In fact, uncertainty analysis has been heavily analyzed in robotics [1] and rigid Structure from Motion (SfM) [2] [3] as researchers realize that the noise in the observation is innegligible. The uncertainty quantification of the estimated state provides important statistical descriptions

Jingwei Song and Mitesh Patel is with the FXPAL, Palo Alto, California 94304, USA. e-mail: (jsong,mitesh@fxpal.com).

for further applications like quality assessment, localization, mapping, path planning, and multi-source information fusion. The estimated state and the associated uncertainty are adopted in these applications. In traditional rigid SfM and robotic applications, the state, as well as the uncertainty, are inferred from the measurements with noises in the modeled state transitional process. Denote the state \mathbf{X} as the set of the camera pose and the feature positions. Each element of the corresponding observation $f(\mathbf{X})$ follows the Gaussian distribution $\mathbf{O}_i \sim \mathcal{N}(\mu, \sigma^2)$, where μ is the mean and σ is the standard deviation. After minimizing the observation errors $\sum f(\mathbf{X}) - \mathbf{O}$, the uncertainty of the objective function is obtained as:

$$Cov(\mathbf{X}^d) = \left[\frac{\partial f(\mathbf{X}^d)}{\mathbf{X}^d} \right]^\top \Delta \left[\frac{\partial f(\mathbf{X}^d)}{\mathbf{X}^d} \right], \quad (1)$$

where Δ is the covariance matrix of the observation \mathbf{O} , and is composed of diagonal matrix with each element δ^2 . \mathbf{X}^d is the optimized state.

The NRSfM community, however, lacks the uncertainty analysis. It may be attributed to the difficulty in linearizing the objective function or the discontinuity of the objective function. Unlike in the field of robotics and SfM where the sensor-to-object functions are easy to be linearized locally, the NRSfM involves either factorization or nuclear norm minimization, which hinders the process in Eq. (1). The goal of this research is to overcome this issue by proposing a general uncertainty quantification for both factorization and nuclear norm formulations.

In this paper, we propose a practical solution to the element-wise uncertainty quantification in SDP based NRSfM. Extensive experiments show that the proposed covariance matrix describes the uncertainty well, and can be applied in measuring confidence intervals of the 3D deformable shape recovered from noisy observations. To be consistent with prior free, specifically rank number free, in SDP based NRSfM, we propose an empirical approximate rank estimation method, and also shows the rank has a remarkably small impact on covariance matrix estimation. Novelties are:

- We propose a closed-form element-wise uncertainty quantification algorithm for the state-of-art low-rank SDP approach.
- A numerical rank estimation method is presented to define the best rank for the confidence interval.

II. LITERATURE REVIEW

A. Review of NRSfM

Following the approach of rigid SfM, early works [4] directly adopt factorization to recover the time-varying 3D

shapes. Later, [5] shows ambiguous solvability in NRSfM that factorization alone is insufficient to solve the ill-posed NRSfM problem. From then on, priors are introduced to constrain the problem into a low-rank subspace to ensure the solvability. The low-rank priors include base shape [6] [7], base trajectory [8] [9] [6], based shape-trajectories [10] [11] [12] and force model [13]. There is a duality in formulation of all the proposed base prior, that is the estimated state (shape or trajectory) is a linear combination of all bases. The differences of these approach lies in the strategy of solving the problem like ‘coarse-to-fine’ [6], probabilistic principle component analysis [7], kernel trick [10] and procrustean analysis in consecutive shapes [14]. As [15] points out, the internal constraint orthonormality of camera orientation and external constraint base shape enables the unique shape structure with the number of basis fixed.

One milestone is achieved by [16] and [17] who enforce low-rank constraint for spatial-temporal smoothness of shape. These approaches push low-rank bases toward spanning the model with a union of low dimensional shape subspace [18] [19] [20]. Conventional bases constraint is substituted with low-rank (nuclear norm for the convexity) minimization. Prior knowledge, specifically the number of bases, is not essential for shape recovery. The automatic prior-free SDP achieves high accuracy with fewer parameter configuration. SDP, together with its derivatives, is the most efficient algorithm in the state-of-art NRSfM community. Following researches include the augmented Lagrange multiplier [21] [22] and union of subspaces [18] [19] [20] for multiple body reconstruction.

In addition to the above-mentioned methods, deep learning [23] [24] is introduced recently in this geometric problem which claims to enable interpretable deformable 3D shape recovery. These approaches encode prior assumptions for representing 3D geometry as patterns that are similar to the low-rank based priors in geometry approaches. The neural network structure falls out of the scope of this paper and we only focus on conventional geometric based formulation.

B. Uncertainty quantification in rigid 3D shape recovery

Another important topic is the quantitative assessment of the reliability of the solution. SfM and SLAM address not only the solution but also the related confidence intervals [25]. In SfM or Simultaneous Localization and Mapping (SLAM), uncertainty is defined as the impact of perturbation of observation, and is often represented as a covariance matrix. Most of the formulations are non-rigid due to the rotation/projection matrix in $SO(3)$. Therefore, in batch camera poses and feature positions estimation, SfM, and SLAM routinely linearize the objective function locally and solve it with the least square state estimation [26], which defines the covariance as the inverse of the second-order derivations termed as ‘Hessian matrix’. Numerically, the Hessian matrix is often approximated with $\mathbf{H} = \mathbf{J}^\top \mathbf{J}$ where \mathbf{J} is the Jacobian matrix. Similarly, in the sequential state estimation, SLAM [27] propagates the uncertainty through the linearized state propagation function with Extended Kalman Filter (EKF), a nonlinear version of Kalman Filter. With a known initial

pose uncertainty (or presumed) propagated and observation uncertainty, the system balance the weights, defined as the variance, to yield the optimal state estimation as well as the corresponding uncertainty for the next step.

In SDP based NRSfM, however, is far from reaching the straightforward closed-form solutions in SfM or SLAM. Although numerous researches are conducted in rigid cases, no work addresses the uncertainty in NRSfM. SDP fails to pin the formulation down to a closed-form formulation as SLAM or SfM, due to the nonlinear nuclear norm constraint. The factorization or nuclear norm term is an obstruct toward closed-form uncertainty propagation from input to output. Recently, a breakthrough is achieved in optimal uncertainty quantification and inference for noisy matrix completion [28]. It measures the confidence interval by developing simple debiased estimators that admit tractable and accurate distributional characterizations. The relaxed convex optimization in matrix completion shares the similarity in SDP in NRSfM [17]. Therefore, we are inspired by this work and try to provide a solution to quantify the uncertainty of the estimated time-varying shape in the NRSfM scenario. Moreover, [28] only provides a solution to the matrix with an exact low-rank structure, while we aim at providing a solution in NRSfM to allow uncertainty quantification for approximate matrix.

III. METHODOLOGY

A. Problem definition and low-rank solver.

The classic low-rank based NRSfM [17] formulates the shape recovery as minimizing the following objective function:

$$\min_{\mathbf{S}} \mu \|\mathbf{S}^\# \|_* + \frac{1}{2} \|\mathbf{W} - \mathbf{RS}\|_F^2, \text{ such that} \quad (2)$$

$$\mathbf{S}^\# = g(\mathbf{S}) = [\mathbf{P}_X \mathbf{P}_Y \mathbf{P}_Z] (\mathbf{I}_3 \otimes \mathbf{S})$$

$$\mathbf{S} = \begin{pmatrix} x_1^1 & y_1^1 & z_1^1 & \cdots & x_1^F & y_1^F & z_1^F \\ \vdots & \vdots & \vdots & \vdots & \vdots & \vdots & \vdots \\ x_N^1 & y_N^1 & z_N^1 & \cdots & x_N^F & y_N^F & z_N^F \end{pmatrix}^\top, \quad (3)$$

$$\mathbf{S}^\# = \begin{pmatrix} x_1^1 & \cdots & x_N^1 & y_1^1 & \cdots & y_N^1 & z_1^1 & \cdots & z_N^1 \\ \vdots & \ddots & \vdots & \vdots & \ddots & \vdots & \vdots & \ddots & \vdots \\ x_1^F & \cdots & x_N^F & y_1^F & \cdots & y_N^F & z_1^F & \cdots & z_N^F \end{pmatrix}^\top, \quad (4)$$

where the time-varying shape \mathbf{S} (Eq. (3)) is a $3F \times N$ matrix with F frames and N feature points. Eq. (4) shows the definition of $\mathbf{S}^\#$ with the size $3N \times F$. It is the rearranged form of the matrix \mathbf{S} for conciseness. $\|\cdot\|_*$ is the nuclear norm and $\|\cdot\|_F$ is the Frobenius norm. μ is the hyper-parameter balancing two constraints. $\mathbf{S}^\# = g(\mathbf{S})$ maps $\mathbf{S}^\#$ to \mathbf{S} while $\mathbf{S} = g^{-1}(\mathbf{S}^\#)$ does the opposite. $\mathbf{P}_X, \mathbf{P}_Y, \mathbf{P}_Z \in \mathbb{R}^{F \times 3F}$ are some properly defined 0-1-valued ‘row-selection’ matrices (similar to the ‘permutation matrix’). $\mathbf{W} \in \mathbb{R}^{2F \times N}$ is the observation with missing elements.

$$\mathbf{W}_{ij} = \mathbf{W}_{ij}^* + \mathbf{E}_{ij}, \quad \mathbf{E}_{ij} \stackrel{\text{i.i.d.}}{\sim} \mathcal{N}(0, \sigma_0^2), \quad \text{for all } (i, j) \in \Omega, \quad (5)$$

where $\Omega \subseteq \{1, \dots, 2F\} \times \{1, \dots, N\}$ is the subset of indexes, \mathbf{W}^* is the ground truth of the observation. And \mathbf{E}_{ij} denotes

the spatial disturbance of element (ij) in measurement process. σ_0^2 is the variance of the noise.

\mathbf{R} is composed of partial diagonal block matrix as \mathbf{R}_i . \mathbf{R}_i is the first two lines of its complete form $\overline{\mathbf{R}}_i \in SO(3)$. \mathbf{R} defines the 3D ($\mathbf{p}_j^i = [x_j^i \ y_j^i \ z_j^i]$ point j in frame i) to 2D ($\tilde{\mathbf{u}}_j^i$ track j in frame i) projection:

$$\underbrace{\begin{pmatrix} \mathbf{u}_1^1 & \cdots & \mathbf{u}_1^N \\ \vdots & \ddots & \vdots \\ \mathbf{u}_F^1 & \cdots & \mathbf{u}_F^N \end{pmatrix}}_{\mathbf{W}} = \underbrace{\begin{pmatrix} \mathbf{R}_1 & & \\ & \ddots & \\ & & \mathbf{R}_F \end{pmatrix}}_{\mathbf{R}} \underbrace{\begin{pmatrix} \mathbf{p}_1^1 & \cdots & \mathbf{p}_1^N \\ \vdots & \ddots & \vdots \\ \mathbf{p}_F^1 & \cdots & \mathbf{p}_F^N \end{pmatrix}}_{\mathbf{S}}. \quad (6)$$

Camera projection matrix \mathbf{R} and the deforming shape \mathbf{S} are estimated after the factorizing of \mathbf{W} in Eq. (6). There is one constraint termed as the orthographic constraint, $\mathbf{R}^\top \mathbf{R} = \mathbf{I}$ and \mathbf{I} is an identical matrix, is commonly adopted [15]. [15] also shows that the \mathbf{R} is ambiguous while the reconstructed shape is unique with a fixed rank. By imposing the orthographic constraint, conventional NRSfM method adopts rank $3K$ factorization [29] [4], where K is deliberately chosen and results is highly dependent on the value of K .

To overcome the difficulty of selecting the optimal K , the direct method (Eq. (2)) is proposed to constrain the estimated shape to be in low-rank condition. Practically, low-rank constraint makes the objective function nonconvex, thus nuclear norm minimization is adopted to relax the problem to convex [17] [16] [29]. These works demonstrate the efficiency and accuracy of the prior free formulation.

Eq. (7) shows an iterative approach [30] for minimizing the objective function Eq. (2). The nuclear norm is minimized with the shrinkage operator $\mathcal{S}_v(\cdot)$ and the Frobenius norm is minimized with the conventional gradient descendent.

$$\begin{cases} \mathbf{S}^{\sharp(t)} = \mathbf{S}^{\sharp(t)} - \tau \mathcal{G}(\mathbf{S}^{\sharp(t)}) \\ \mathbf{S}^{\sharp(t+1)} = \mathcal{S}_{\tau\mu}(\mathbf{S}^{\sharp(t)}) \end{cases} \quad (7)$$

where Σ_S is the diagonal singular value matrix of $\mathcal{S}_v(\cdot)$. v is the arbitrary threshold for numerically reducing the singularity. The shrinkage operator maps the input matrix by manipulating the diagonal element Σ_{Sii} of Σ_S :

$$\Sigma_{Sii} = \begin{cases} \Sigma_{Sii} - v, & \Sigma_{Sii} > v \\ 0, & |\Sigma_{Sii}| \leq v \end{cases} \quad (8)$$

$\mathcal{G}(\cdot)$ is the gradient matrix and defined as:

$$\mathcal{G}(\mathbf{S}^\sharp) = \frac{\partial \frac{1}{2} \|\mathbf{W} - \mathbf{RS}\|_F^2}{\partial \mathbf{S}^\sharp} = [\mathbf{P}_X \mathbf{P}_Y \mathbf{P}_Z] (\mathbf{I}_3 \otimes (\mathbf{R}^T (\mathbf{RS} - \mathbf{W}))). \quad (9)$$

It should be addressed that Eq. (9) is calculated by estimating $\mathcal{G}(\mathbf{S})$, and then mapped with $\mathbf{S}^\sharp = g(\mathbf{S})$. This is because function $\mathbf{S}^\sharp = g(\mathbf{S})$ only changes the position of each element. Thus $\mathcal{G}(\mathbf{S}^\sharp)$ and $\mathcal{G}(\mathbf{S})$ can be directly rearrange with $g(\cdot)$.

B. Uncertainty estimation with the exact low-rank structure

We first present the exact low-rank uncertainty quantification approach, then extend it to an approximate low-rank version. In the SDP formulation (Eq. (2)), the ground truth of the time-varying deforming shape is in approximate low-rank structure, meaning it is strictly full-rank but has low nuclear norm which can be viewed as the approximated low-rank structure. In this section, we will show that the closed-form uncertainty quantification for the exact low-rank structure can be retrieved with mathematical manipulation and approximation. After the achievement of the closed-form uncertainty quantification of exact low-rank form, a practical approach is presented to extend it to the approximate version.

Denote $\mathbf{S}^{\sharp\star} \in \mathbb{R}^{3N \times F}$ as the optimal (ground truth) rank- r matrix (the exact low-rank structure case). The Singular Value Decomposition (SVD) of $\mathbf{S}^{\sharp\star}$ is $\mathbf{S}^{\sharp\star} = \mathbf{U}^{\sharp\star} \mathbf{\Sigma}^{\sharp\star} \mathbf{V}^{\sharp\star\top}$. We define two auxiliary matrix $\mathbf{X}^{\star} \triangleq \mathbf{U}^{\sharp\star} \mathbf{\Sigma}^{\sharp\star 1/2} \in \mathbb{R}^{3N \times r}$ and $\mathbf{Y}^{\star} \triangleq \mathbf{V}^{\sharp\star} \mathbf{\Sigma}^{\sharp\star 1/2} \in \mathbb{R}^{F \times r}$. Therefore, we have following rules:

$$\begin{aligned} \mathbf{X}^{\sharp\star\top} \mathbf{X}^{\star} &= \mathbf{Y}^{\sharp\star\top} \mathbf{Y}^{\star} = \mathbf{\Sigma}^{\star} \\ \mathbf{S}^{\sharp\star} &= \mathbf{X}^{\star} \mathbf{Y}^{\star\top}. \end{aligned} \quad (10)$$

In conventional NRSfM definition, \mathbf{Y}^{\star} is termed as the basis matrix and \mathbf{X}^{\star} is the associated linear coefficient [8]. With regard to \mathbf{X}^{\star} and \mathbf{Y}^{\star} , we define $\mathbf{X}^d \in \mathbb{R}^{3N \times r}$, $\mathbf{Y}^d \in \mathbb{R}^{F \times r}$ as the estimated shrinkage operator and $\mathbf{S}^{\sharp d} \in \mathbb{R}^{3N \times F}$ as the de-biased operator. The shrinkage operator is nearly equivalent to the de-biased estimator $\mathbf{S}^{\sharp d} \approx \mathbf{X}^d \mathbf{Y}^{d\top}$. Similarly to the definition of Eq. (3) and Eq. (4), the point cloud form of $\mathbf{S}^{\sharp d}$ is \mathbf{S}^d . Following the ambiguity issue in the coefficient and basis matrix raised by [15], an optimal global rotation matrix $\mathbf{H}^d \in \mathbb{R}^{r \times r}$ is needed to rectify $(\mathbf{X}^d, \mathbf{Y}^d)$ to $(\mathbf{X}^{\star}, \mathbf{Y}^{\star})$. We use the following formulation to align them close to the ground truth.

$$\mathbf{H}^d \triangleq \arg \min_{\mathbf{H} \in \mathcal{A}^{r \times r}} \|\mathbf{X}^d \mathbf{H} - \mathbf{X}^{\star}\|_F^2 + \|\mathbf{Y}^d \mathbf{H} - \mathbf{Y}^{\star}\|_F^2, \quad (11)$$

where $\mathcal{A}^{r \times r}$ denotes the set of orthogonal matrix in $\mathbb{R}^{r \times r}$.

Theorem 1. For the estimated operator \mathbf{X}^d and \mathbf{Y}^d , error of the rectified \mathbf{X}^d and \mathbf{Y}^d is:

$$\begin{aligned} \mathbf{X}^d \mathbf{H}^d - \mathbf{X}^{\star} &= \mathbf{Z}_X + \mathbf{\Psi}_X \\ \mathbf{Y}^d \mathbf{H}^d - \mathbf{Y}^{\star} &= \mathbf{Z}_Y + \mathbf{\Psi}_Y. \end{aligned} \quad (12)$$

The row of the error matrices $\mathbf{Z}_X \in \mathbb{R}^{3N \times r}$ (resp. $\mathbf{Z}_Y \in \mathbb{R}^{n \times r}$) are independent and obeys:

$$\begin{aligned} \mathbf{Z}_X^{\top} \mathbf{e}_j &\stackrel{i.i.d.}{\sim} \mathcal{N}(0, \sigma_0^2 (\mathbf{\Sigma}^{\star})^{-1}), & \text{for } 1 \leq j \leq 3N \\ \mathbf{Z}_Y^{\top} \mathbf{e}_j &\stackrel{i.i.d.}{\sim} \mathcal{N}(0, \sigma_0^2 (\mathbf{\Sigma}^{\star})^{-1}), & \text{for } 1 \leq j \leq 3N \end{aligned} \quad (13)$$

where \mathbf{e}_j is the basis vector and $\mathbf{\Psi}_X, \mathbf{\Psi}_Y \in \mathbb{R}^{3N \times r}$ are the residual matrices. Please refer to Section VI for the prove of **theorem 1**. $\mathbf{\Psi}_X$ and $\mathbf{\Psi}_Y$ are significantly smaller than \mathbf{Z}_X and \mathbf{Z}_Y and Eq. (12) is approximated to:

$$\begin{aligned} \mathbf{X}^d \mathbf{H}^d - \mathbf{X}^{\star} &\approx \mathbf{Z}_X \\ \mathbf{Y}^d \mathbf{H}^d - \mathbf{Y}^{\star} &\approx \mathbf{Z}_Y. \end{aligned} \quad (14)$$

Assuming that the first-order expansion is reasonably tight, the element-wise error between the estimation $\mathbf{S}_{ij}^{\#d}$ and the ground truth $\mathbf{S}_{ij}^{\#*}$ are:

$$\begin{aligned}
\mathbf{S}_{ij}^{\#d} - \mathbf{S}_{ij}^{\#*} &= [\mathbf{X}^d \mathbf{H}^d (\mathbf{Y}^d \mathbf{H}^{d\top}) - \mathbf{X}^* \mathbf{Y}^{*\top}]_{ij} \\
&= [\mathbf{e}_i^T \mathbf{X}^d \mathbf{H}^d (\mathbf{Y}^d \mathbf{H}^{d\top}) \mathbf{e}_j - \mathbf{e}_i^T (\mathbf{X}^* \mathbf{Y}^{*\top}) \mathbf{e}_j] \\
&\approx [\mathbf{e}_i^T (\mathbf{X}^d \mathbf{H}^d - \mathbf{X}^*) \mathbf{Y}^{*\top} \mathbf{e}_j + \mathbf{e}_i^T \mathbf{X}^* (\mathbf{Y}^d \mathbf{H}^d - \mathbf{Y}^{*\top}) \mathbf{e}_j] \\
&\approx [\mathbf{e}_i^T (\mathbf{Z}_X \mathbf{Y}^{*\top}) \mathbf{e}_j + \mathbf{e}_i^T (\mathbf{X}^* \mathbf{Z}_Y^{\top}) \mathbf{e}_j]
\end{aligned} \tag{15}$$

where the bases $\mathbf{e}_i, \mathbf{e}_j$ picks the elements involved in calculating element in position (i, j) , $[\cdot]_{ij}$ is the (i, j) element of \cdot . After some manipulation, we have the variance of the error as:

$$\begin{aligned}
\text{Var}(\mathbf{S}_{ij}^{\#d} - \mathbf{S}_{ij}^{\#*}) &\stackrel{(i)}{\approx} [\text{Var}(\mathbf{e}_i^T (\mathbf{Z}_X \mathbf{Y}^{*\top}) \mathbf{e}_j) + \text{Var}(\mathbf{e}_i^T (\mathbf{X}^* \mathbf{Z}_Y^{\top}) \mathbf{e}_j)] \\
&\stackrel{(ii)}{=} \sigma_0^2 [\mathbf{e}_i^T \mathbf{Y}^* (\Sigma^*)^{-1} \mathbf{Y}^{*\top} \mathbf{e}_j + \mathbf{e}_i^T \mathbf{X}^* (\Sigma^*)^{-1} \mathbf{X}^{*\top} \mathbf{e}_i] \\
&\stackrel{(iii)}{=} \sigma_0^2 (\|\mathbf{U}_{i,:}^*\|_2^2 + \|\mathbf{V}_{j,:}^*\|_2^2)
\end{aligned} \tag{16}$$

where (i) is from the **Theorem 1** since \mathbf{Z}_X and \mathbf{Z}_Y are nearly independent. (ii) is from the Eq. (12). (iii) $\mathbf{U}_{i,:}^*$ and $\mathbf{V}_{j,:}^*$ are the i/j th row of \mathbf{U}^* and \mathbf{V}^* . For simplicity, we define $v_{ij}^* = (\|\mathbf{U}_{i,:}^*\|_2^2 + \|\mathbf{V}_{j,:}^*\|_2^2)$. The covariance is converted to:

$$\text{Var}(\mathbf{S}_{ij}^{\#d} - \mathbf{S}_{ij}^{\#*}) \approx \sigma_0^2 v_{ij}^* \tag{17}$$

In practice, the ground truth $\mathbf{U}_{i,:}^*$ and $\mathbf{V}_{j,:}^*$ is impossible to estimate, we approximate them with the estimated version $\mathbf{U}_{i,:}^d$ and $\mathbf{V}_{j,:}^d$.

$$\text{Var}(\mathbf{S}_{ij}^{\#d} - \mathbf{S}_{ij}^{\#*}) \approx \sigma_0^2 (\|\mathbf{U}_{i,:}^d\|_2^2 + \|\mathbf{V}_{j,:}^d\|_2^2) = \sigma_0^2 v_{ij}^d \tag{18}$$

where $\sigma_0^2 v_{ij}^d$ can be regarded as the estimated version of $\sigma_0^2 v_{ij}^*$. $\mathbf{U}_{i,:}^d$ and $\mathbf{V}_{j,:}^d$ are the i/j th row of \mathbf{U}^d and \mathbf{V}^d . Therefore, the corresponding variance of \mathbf{S}^d is Eq. (19) providing a closed form solution to the estimation in the scenario of exact low-rank NRSfM case.

$$\text{Var}(\mathbf{S}_{ij}^d - \mathbf{S}_{ij}^{\#*}) \approx g(\sigma_0^2 v_{ij}^d) \tag{19}$$

C. Defining the optimal rank for uncertainty

This section aims at achieving approximate low-rank NRSfM quantification based on the closed-form solution of the exact low-rank NRSfM scenario demonstrated in Section III-B. As [31] points out, the closed-form solution to approximate low-rank uncertainty quantification in matrix completion problem remains difficult; this also applies to approximate low-rank formulation in NRSfM scenario. Many previous researches in NRSfM point out that the structure of shape $\mathbf{S}^{\#}$ is a typical approximate low-rank matrix [17] [21].

We propose that the approximate low-rank shape uncertainty quantification can be approximated with the exact version and a chosen rank r . Naively, r may be estimated by analyzing the shape $\mathbf{S}^{\#d}$ with some threshold. However, the noisy observation

Algorithm 1: Algorithm of SDP and uncertainty quantification.

Input: Complete or incomplete 2D trajectories \mathbf{W} and hyper parameters
Output: Camera projection \mathbf{R} , 3D reconstruction \mathbf{S}^d and corresponding element-wise variance $\text{Var}(\mathbf{S}_{ij}^d - \mathbf{S}_{ij}^{\#*})$

- 1 Estimate camera projection \mathbf{R}
- 2 $i = 1$
- 3 $\mathbf{S} = \text{PINV}(\mathbf{R})\mathbf{W}$
- 4 $\mathbf{S}^{\#} = g^{-1}(\mathbf{S})$
- 5 **while** $i < i_{max}$ **do**
- 6 **while** not converged **do**
- 7 /* Update model parameter */
- 8 $\mathbf{S}^{\#} = \mathcal{S}_{\tau\mu}(\mathbf{S}^{\#})$
- 9 $\mathbf{S}_r^{\#} = \mathbf{S}^{\#}$
- 10 $\mathbf{S} = g(\mathbf{S}^{\#})$
- 11 $\mathcal{G}(\mathbf{S}^{\#}) = [\mathbf{P}_X \mathbf{P}_Y \mathbf{P}_Z] (\mathbf{I}_3 \otimes (\mathbf{R}^T (\mathbf{R}\mathbf{S} - \mathbf{W})))$
- 12 $\mathbf{S}^{\#} = \mathbf{S}^{\#} - \tau \mathcal{G}(\mathbf{S}^{\#})$
- 13 /* Update penalty weights */
- 14 $\tau = \max(\mu\eta_{\mu}^i, 10^{-10})$
- 15 /* Check Convergence */
- 16 $\|\mathbf{W} - \mathbf{R}\mathbf{S}\|_{\infty} < \epsilon$
- 17 **end**
- 18 $i = i + 1$
- 19 **end**
- 20 $\mathbf{S}^d = \mathbf{S}$
- 21 $\mathbf{U}^d \Sigma^d \mathbf{V}^{d\top} = \text{SVD}(\mathbf{S}_r^{\#})$
- 22 $\text{Var}(\mathbf{S}_{ij}^d - \mathbf{S}_{ij}^{\#*}) \approx g(\sigma_0^2 v_{ij}^d)$

Notation: $\text{SVD}(\cdot)$ implements the SVD factorization.
 $\text{PINV}(\cdot)$ is the MoorePenrose inverse.

TABLE I: Numerical test of the relations between noise and the optimal rank. The optimal rank is tested with regard to the ground truth.

	0.01	0.05	0.08	0.1
Optimal rank	0.1	0.9554	0.0258	75

increases the complexity of the observation \mathbf{W} leading to the larger nuclear norm in the optimized state $\mathbf{S}^{\#d}$ than the ground truth $\mathbf{S}^{\#*}$. **Thus the determination of rank r is difficult.**

Remark 1. The rank (nuclear norm) of the estimated shape increases as noise magnifies on condition that the weight balance μ is fixed. In the case of noisy observations, $\mathbf{S}^{\#d}$ needs higher dimensions, or higher nuclear norm, to allow fitting the noisy observation \mathbf{W} . With the same estimated state, the reprojection error term with noisy observation \mathbf{W} is greater than the term without noisy observation ($\frac{1}{2} \|\mathbf{W} - \mathbf{R}\mathbf{S}\|_{\text{F}}^2 > \frac{1}{2} \|\mathbf{W}^* - \mathbf{R}\mathbf{S}\|_{\text{F}}^2$). The state \mathbf{S} inevitably needs adjustment to minimize the reprojection error term. This claim will be numerically validated in Section IV.

We address the optimal rank r by introducing an approximate solution. In the t th iterative SDP solver in Eq. (7), the shrinkage operator (Eq. (8)) reduces the nuclear norm to its

TABLE II: Coverage rates of $\text{Var}(\mathbf{S}_{ij}^d - \mathbf{S}_{ij}^*)$ for different σ_0 over 100 Monte Carlo trials. ‘std’ denotes the standard deviation. The value is the statistical results over all elements of the 4 datasets.

	σ_0	Mean	Std	rank
MoCap	0.01	0.9188	0.0673	11
	0.05	0.9493	0.0381	25
	0.08	0.9375	0.0483	61
	0.1	0.9554	0.0258	75

new state $\mathbf{S}^{\#(t+1)}$. When the algorithm converges, we assumes the state $\mathbf{S}^{\#(t+1)}$ in the subspace with rank r is close to the corresponding local minima. And the distance is close enough that the rank of $\mathbf{S}^{\#(t+1)}$ can be approximated as the optimal rank. Since the final optimized $\mathbf{S}^{\#d}$ is an approximate low-rank matrix and the rank if almost full, we can only substitute the optimal rank with its nearest subspace. The last few steps in searching local local minima $\mathbf{S}^{\#d}$ around its surrounding space provide a good way for approximating.

Algorithm 1 presents the technical details for estimating \mathbf{S}^d and the associated uncertainty from the observed 2D trajectories \mathbf{W} based on the SDP formulation defined in Eq. (2). The minimizing approach strictly follows the original SDP provided by [17], while we couple it with the proposed closed-form uncertainty quantification approach. Moreover, for the camera projection matrix \mathbf{R} , we follow conventional approaches [8] [21] by solving it independently. We encode it as standard least square formulation and solve with Gauss-Newton formulation, with the projection constraint $\mathbf{W} = \mathbf{RS}$ and orthonormality constraint $\mathbf{I}_{2F} = \mathbf{RR}^\top$. \mathbf{I}_{2F} is the identical matrix with size $2F$.

IV. RESULTS AND DISCUSSION

The proposed method is validated quantitatively on several different scenarios in the MoCap dataset provided by CMU [32]. The MoCap dataset uses more than 30 markers distributed on the skeleton of the human body. Accurate 3D marker positions of human body motions are tracked by an infrared camera. It is a widely used dataset for validation in computer vision community [21] [17] [22]. Four widely tested dataset used in [15] is adopted, which projects the original 3D points on the 2D space with an orthographic camera following a relative circular motion around the object, at an stable angular speed. Among them, four popular datasets, ‘Drink’ (1102/41), ‘Pickup (357/41)’, ‘Yoga (307/41)’, ‘Stretch (370/41)’ are used. Where (F/N) is the number of frames F and the number of tracked points N . Fig. 1 shows some sample results of the reconstruction.

A. Uncertainty quantification

We conduct Monte Carlo tests with different level of noises over the 2D observations. Fig. 2 shows the samples of the four datasets in SDP process following Algorithm 1. For each dataset, Gaussian noise is imposed on the 2D tracked points with different standard deviation σ_0 . All parameter settings follow original SDP approach [17] including $i_{\max} = 20$, $\mu = 4$,

TABLE III: The probability values (p -value) of the Shapiro-Wilk test of \mathbf{S}_{11} , \mathbf{S}_{34} , \mathbf{S}_{58} and \mathbf{S}_{69} . The p -value > 0.05 indicates a significant possibility that \mathbf{S}_{ij} is normally distributed.

δ_0	Element	\mathbf{S}_{11}	\mathbf{S}_{34}	\mathbf{S}_{58}	\mathbf{S}_{69}
0.01	0.01	0.5429	0.4494	0.3911	0.7230
	0.05	0.7572	0.0133	0.0645	0.2913
	0.08	0.0453	0.8791	0.2747	0.3703
	0.1	0.0282	0.4147	0.6258	0.2979

$\eta_\mu = 0.25$ and $\epsilon = 10^{-10}$. We perform Monte Carlo test of 100 time on each dataset with a given σ_0 . For each test, the element wise mean values $\mathbf{S}_{ij}^{\#d}$ is calculated. For each element in trial k , the error is defined as

$$e_{ij}^k = \text{abs}(\mathbf{S}_{ij}^{\#d} - \overline{\mathbf{S}_{ij}^{\#d}}), \quad k \in [1, \dots, 100] \quad (20)$$

where $\text{abs}(\cdot)$ is the absolute value. Ideally, if e_{ij}^k follows normal distribution and our variance $\sigma_0^2 v_{ij}^d$ is correct, 95% of e_{ij}^k will fall within the range of $\overline{\mathbf{S}_{ij}^{\#d}} \pm 1.96\sigma\sqrt{v_{ij}^d}$. Thus we define the average rate as the ratio of e_{ij}^k fall into $1.96\sigma\sqrt{v_{ij}^d}$ and presents the result in Table II. Table II presents the general statistical results over all elements of the 4 datasets, and it indicate that the closed-form uncertainty quantification coverage rate is close to 95%. Moreover, Table II also validates our claim in Section III-C that the optimal rank of the NRSfM is highly influenced with the noise.

To further address the uncertainty quantification for individual point, we present the Table III to validate the normal distribution of the result. The p -value indicates that 14 out of 16 samples are significantly in the normal distribution. Since all elements of the shape should be consistent (either obey or reject the normal distribution), we can conclude that the shape obeys the normal distribution. The two samples that reject this assumption in higher possibility may be attributed to small sample of training sets.

In addition to the general coverage rate of the proposed uncertainty estimation approach, we also intend to validate that the estimated shape $\mathbf{S}^{\#d}$ follows the Gaussian distribution. We show the quantile-quantile (Q-Q) plots (Fig. 2) of $\mathbf{S}_{11}^{\#d}$ (dataset ‘drink’), $\mathbf{S}_{34}^{\#d}$ (dataset ‘pickup’), $\mathbf{S}_{58}^{\#d}$ (dataset ‘stretch’) and $\mathbf{S}_{69}^{\#d}$ (dataset ‘yoga’) in the case of $\sigma_0 = 0.08$ against the standard normal distribution. Two more Q-Q plots of surgical data are also presented. In the figure, all 100 elements in the Monte Carlo tests are presented.

B. Robustness of the approximate low-rank estimation

On top of the coverage rate tests, we further validate that the proposed approach is robust to the rank estimated from the local minima. Numerically, the $v_{ij} \in [0, 2]$ is dependent on the numerical rank as it is 0 when the matrix is null while 2 when it is full-rank. We deliberately tests different rank in step 19 in Algorithm 1 and show that the proposed approach is not sensitive to the numerical rank estimation.

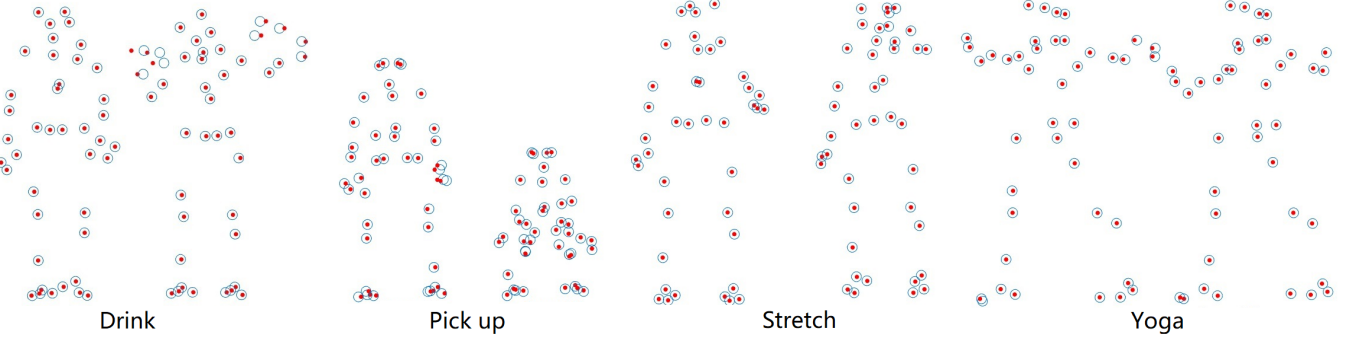


Fig. 1: Illustrated are the sample results of the surgical dataset.

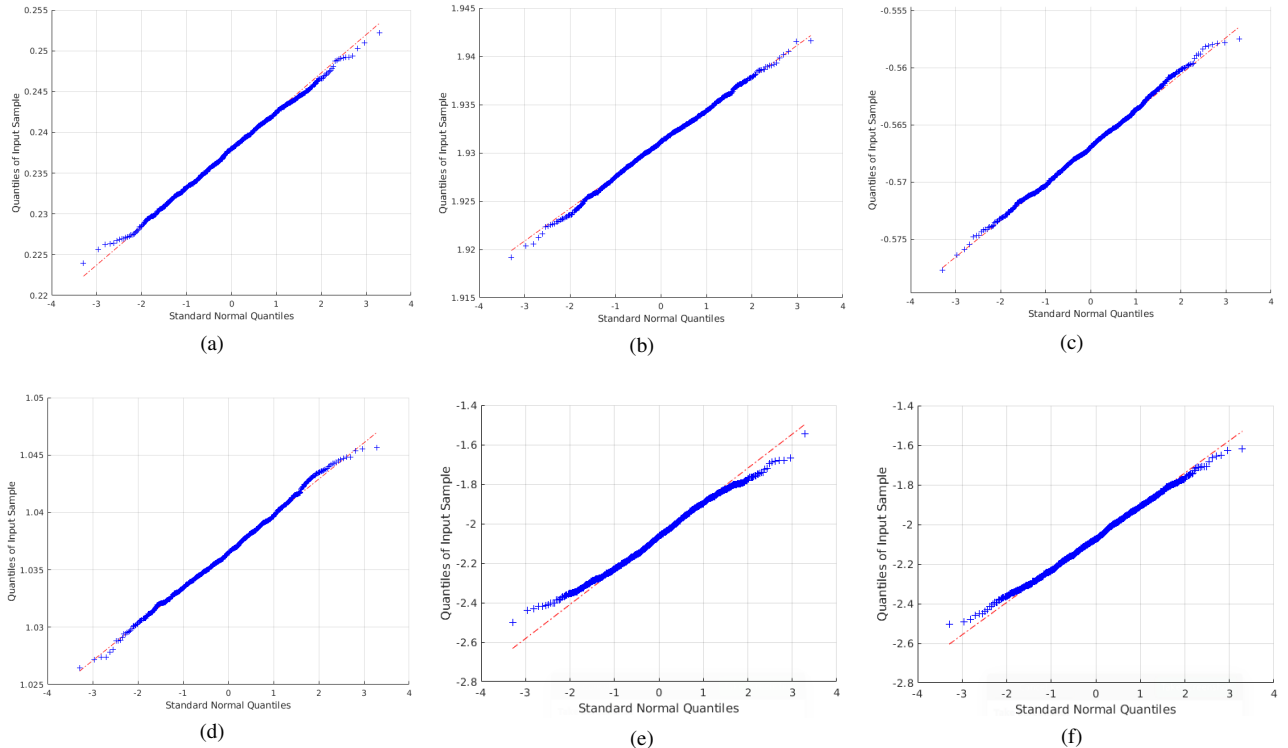


Fig. 2: Illustrated are the Q-Q (quantile-quantile) plot of S_{11} , S_{34} , S_{58} and S_{69} against the standard normal distribution in (a), (b), (c) and (d) respectively. They are over 100 independent trials for noise $\sigma_0 = 0.08$ in the four data ‘drink’, ‘pickup’, ‘stretch’ and ‘yoga’. (e) and (f) shows the Q-Q plot with $\sigma_0 = 1$.

Table IV illustrates the coverage rate with different disturbance on the rank numerically estimated in Algorithm 1. Among the 16 tests, 10 achieves 2% error and 12 achieves 3% error with regard to the 95% ground truth. Moreover, comparing the standard deviation with table II, there is no significant difference. Therefore, the presented uncertainty quantification approach is robust to the potential different optimal rank in numerical estimation process.

V. CONCLUSION

This is the first research address the uncertainty quantification in NRSfM problems. We propose a closed-form element-wise uncertainty quantification algorithm for the state-of-art

low-rank based SDP approach. The proposed method only requires the statistical distribution of the 2D observation. To overcome the approximate low-rank structure of the time-varying shape, we present a numerical approach to estimate the optimal rank and convert the problem from approximate low-rank recovery to exact low-rank recovery. Monte carlo tests validate that the coverage rate of the element-wise variance describes the distribution of the estimated time-varying shape precisely. Furthermore, robustness tests demonstrate that the uncertainty is not sensitive to the rank estimated with our modified SDP workflow. Our closed-form uncertainty quantification approach can be applied in practical scenarios.

TABLE IV: Presented is the robustness test of the coverage rate over different rank. We exert $m\% \in [-10, -20, 10, 20]$ percentage error over the rank, and test the coverage rates of $\text{Var}(\mathbf{S}_{ij}^d - \mathbf{S}_{ij}^*)$ for different σ_0 over 100 Monte Carlo trials.

σ_0	+10%		+20%		-10%		-20%	
	Mean	Std	Mean	Std	Mean	Std	Mean	Std
0.01	0.9303	0.0603	0.9408	0.0543	0.9018	0.0791	0.8871	0.0832
0.05	0.9611	0.0312	0.9671	0.0273	0.9393	0.0438	0.9196	0.0540
0.08	0.9479	0.0425	0.9564	0.0374	0.9245	0.0547	0.9080	0.0617
0.1	0.9649	0.0216	0.9713	0.0184	0.9448	0.0302	0.9290	0.0361

VI. APPENDIX

Proof of Theorem 1. With regard to the objective function Eq. (2), the optimized shrinkage optimizer \mathbf{X}^d , \mathbf{Y}^d should satisfy the minimum of $f(\mathbf{X}^d, \mathbf{Y}^d)$:

$$\begin{aligned} \min f(\mathbf{X}^d, \mathbf{Y}^d) &= \frac{1}{2} \|\mathbf{W} - \mathbf{R}\mathbf{S}^d\|_F^2, \text{ such that} \\ \mathbf{S}^{\#d} &= g(\mathbf{S}^d) = [\mathbf{P}_X \mathbf{P}_Y \mathbf{P}_Z] (\mathbf{I}_3 \otimes \mathbf{S}^d) \\ \mathbf{S}^{\#d} &= \mathbf{X}^d \mathbf{Y}^{d\top} \end{aligned} \quad (21)$$

$f(\mathbf{X}^d, \mathbf{Y}^d)$ is close to global minimum $f(\mathbf{X}^*, \mathbf{Y}^*)$ meaning the first-order expansion is close to zero matrix defined as O .

$$\begin{aligned} \frac{\partial f(\mathbf{X}^d, \mathbf{Y}^d)}{\partial \mathbf{X}^d} &\stackrel{(i)}{=} g(\mathbf{S}^d - \mathbf{R}^\top \mathbf{W}) \mathbf{Y}^d \\ &= g(\mathbf{S}^d - \mathbf{R}^\top (\mathbf{W}^* + \mathbf{E})) \mathbf{Y}^d \\ &= g(\mathbf{S}^d - \mathbf{R}^\top (\mathbf{R}\mathbf{S}^* + \mathbf{E})) \mathbf{Y}^d \\ &= g(\mathbf{S}^d - \mathbf{S}^* - \mathbf{R}^\top \mathbf{E}) \mathbf{Y}^d \\ &= (\mathbf{X}^d \mathbf{Y}^{d\top} - \mathbf{X}^* \mathbf{Y}^{*\top} - g(\mathbf{R}^\top \mathbf{E})) \mathbf{Y}^d \\ &\stackrel{(ii)}{\approx} (\mathbf{X}^d \mathbf{Y}^{d\top} - \mathbf{X}^* \mathbf{Y}^{*\top} - g(\mathbf{R}^\top \mathbf{E})) \mathbf{Y}^d \approx O, \end{aligned} \quad (22)$$

$$\begin{aligned} \frac{\partial f(\mathbf{X}^d, \mathbf{Y}^d)}{\partial \mathbf{Y}^d} &\stackrel{(i)}{=} \mathbf{X}^{d\top} g(\mathbf{S}^d - \mathbf{R}^\top \mathbf{W}) \\ &= \mathbf{X}^{d\top} g(\mathbf{S}^d - \mathbf{R}^\top (\mathbf{W}^* + \mathbf{E})) \\ &= \mathbf{X}^{d\top} g(\mathbf{S}^d - \mathbf{R}^\top (\mathbf{R}\mathbf{S}^* + \mathbf{E})) \\ &= \mathbf{X}^{d\top} g(\mathbf{S}^d - \mathbf{S}^* - \mathbf{R}^\top \mathbf{E}) \\ &= \mathbf{X}^{d\top} (\mathbf{X}^d \mathbf{Y}^{d\top} - \mathbf{X}^* \mathbf{Y}^{*\top} - g(\mathbf{R}^\top \mathbf{E})) \\ &\stackrel{(ii)}{\approx} \mathbf{X}^{d\top} (\mathbf{X}^d \mathbf{Y}^{d\top} - \mathbf{X}^* \mathbf{Y}^{*\top} - g(\mathbf{R}^\top \mathbf{E})) \approx O, \end{aligned} \quad (23)$$

(i) is resulted from Eq. (9) and $d\mathbf{S}^{\#d} = d\mathbf{X}^d \mathbf{Y}^{d\top} + \mathbf{X}^d (d\mathbf{Y}^d)^\top$

(ii) is approximated by the fact that $\mathbf{X}^d/\mathbf{Y}^d$ are the optimized state and should be close to $\mathbf{X}^*/\mathbf{Y}^*$. We manipulate Eq. (22) and Eq. (23) to:

$$\begin{aligned} (\mathbf{X}^d - \mathbf{X}^*) \mathbf{Y}^{d\top} \mathbf{Y}^d &\approx g(\mathbf{R}^\top \mathbf{E}) \mathbf{Y}^d \\ (\mathbf{X}^d - \mathbf{X}^*) &\approx g(\mathbf{R}^\top \mathbf{E}) \mathbf{Y}^d (\mathbf{Y}^{d\top} \mathbf{Y}^d)^{-1} \\ (\mathbf{X}^d - \mathbf{X}^*) \mathbf{e}_j &\approx g(\mathbf{R}^\top \mathbf{E}) \mathbf{Y}^d (\mathbf{Y}^{d\top} \mathbf{Y}^d)^{-1} \mathbf{e}_j \stackrel{(i)}{\sim} \mathcal{N}(0, \sigma_0^2 (\Sigma^*)^{-1}), \end{aligned} \quad (24)$$

$$\begin{aligned} \mathbf{X}^d (\mathbf{Y}^{d\top} - \mathbf{Y}^{*\top}) \mathbf{X}^{d\top} &\approx g(\mathbf{R}^\top \mathbf{E}) \mathbf{X}^{d\top} \\ \mathbf{X}^{d\top} \mathbf{X}^d (\mathbf{Y}^d - \mathbf{Y}^*) &\approx \mathbf{X}^d g(\mathbf{R}^\top \mathbf{E})^\top \\ (\mathbf{Y}^d - \mathbf{Y}^*) \mathbf{e}_j &\approx (\mathbf{X}^{d\top} \mathbf{X}^d)^{-1} \mathbf{X}^d g(\mathbf{R}^\top \mathbf{E})^\top \mathbf{e}_j \stackrel{(i)}{\sim} \mathcal{N}(0, \sigma_0^2 (\Sigma^*)^{-1}), \end{aligned} \quad (25)$$

The prove of step (i): Let us first define $\hat{\mathbf{E}} \triangleq g(\mathbf{R}^\top \mathbf{E})$ and show $\hat{\mathbf{E}}$ is in the probability of $\mathcal{N}(0, \sigma_0^2)$. The definition of \mathbf{R} is a block diagonal matrix with each diagonal block \mathbf{R}_i is a 3×2

rotation matrix. We divide \mathbf{E} into 1×2 vector and denoted as \mathbf{E}_{ij} where $i \subseteq \{1, \dots, F\}$ and $j \subseteq \{1, \dots, N\}$. For each $\bar{\mathbf{E}}_{ij}$, there is corresponding 1×3 vector $\bar{\mathbf{E}}_{ij} = [\mathbf{E}_{ij} \ 0]^\top$ while \mathbf{R}_i is converted to its complete rotation matrix $\bar{\mathbf{R}}_i$ in 3×3 . The product is:

$$\mathbf{V}_{ij} = \bar{\mathbf{R}}_i^\top \bar{\mathbf{E}}_{ij} \quad (26)$$

Since the probability of $\bar{\mathbf{E}}_{ij}$ is isotropic and rotation $\bar{\mathbf{R}}_i$ is a rigid global rotation, the probability of \mathbf{V}_{ij} is also isotropic and has the same statistical distribution as $\bar{\mathbf{E}}_{ij}$. Thus $\mathbf{R}_k^\top \bar{\mathbf{E}}_{ij}$ shares the same probability as \mathbf{E}_{ij} . Similar to the full version shown in Eq. (26), the product $\mathbf{R}^\top \mathbf{E} \sim \mathcal{N}(0, \sigma^2)$. Therefore, considering $g(\cdot)$ is only rearranging elements, **matrix $\hat{\mathbf{E}} = g(\mathbf{R}^\top \mathbf{E})$ shares the same probability as \mathbf{E} , with the probability $\hat{\mathbf{E}} \sim \mathcal{N}(0, \sigma^2)$.**

Moreover, since $(\mathbf{X}^{d\top} \mathbf{X}^d)^{-1} = (\mathbf{Y}^{d\top} \mathbf{Y}^d)^{-1} = (\Sigma^d)^{-1}$ and $(\Sigma^d)^{-1}$ is a diagonal matrix, each element of $(\Sigma^d)^{-1}$ equals to $1/\|\mathbf{X}_{j..}\|_2^2$ or $1/\|\mathbf{Y}_{j..}\|_2^2$ where $\mathbf{X}_{j..}^d$ or $\mathbf{Y}_{j..}^d$ is the j th row of matrix \mathbf{X}^d or \mathbf{Y}^d .

With the above conclusion, we prove (i) using \mathbf{X}^d as an example.

$$\begin{aligned} &(\mathbf{X}^{d\top} \mathbf{X}^d)^{-1} \mathbf{X}^d g(\mathbf{R}^\top \mathbf{E})^\top \mathbf{e}_j \\ &= \left[\sum_{i=1}^r \frac{1}{\|\mathbf{X}_{j..}^d\|_2^2} \mathbf{X}_{ji}^d \hat{\mathbf{E}}_{1i}^d \dots \sum_{i=1}^r \frac{1}{\|\mathbf{X}_{j..}^d\|_2^2} \mathbf{X}_{ji}^d \hat{\mathbf{E}}_{ri}^d \right] \end{aligned} \quad (27)$$

Thus, the corresponding variance for each element in Eq. (27) is:

$$\begin{aligned} \text{Var} \left(\sum_{i=1}^r \frac{1}{\|\mathbf{X}_{j..}^d\|_2^2} \mathbf{X}_{ji}^d \hat{\mathbf{E}}_{1i}^d \right) &= \left(\sum_{i=1}^r \frac{1}{\|\mathbf{X}_{j..}^d\|_2^2} \mathbf{X}_{ji}^d \right)^2 \sigma_0^2 \\ &= \frac{1}{(\|\mathbf{X}_{j..}^d\|_2^2)^2} \left(\sum_{i=1}^r \mathbf{X}_{ji}^d \right)^2 \sigma_0^2 \\ &= \frac{\|\mathbf{X}_{j..}^d\|_2^2}{\|\mathbf{X}_{j..}^d\|_2^4} \sigma_0^2 \\ &= (\Sigma_{jj}^d)^{-1} \sigma_0^2 \end{aligned} \quad (28)$$

The same prove applies to $(\mathbf{X}^d - \mathbf{X}^*) \mathbf{e}_j \sim \mathcal{N}(0, \sigma^2 (\Sigma^*)^{-1})$. This concludes the proof of (i) and also the proof of **theorem 1**.

REFERENCES

- [1] S. Thrun, W. Burgard, and D. Fox, *Probabilistic robotics*. MIT press, 2005.
- [2] M. Irani and P. Anandan, “Factorization with uncertainty,” in *European Conference on Computer Vision*, pp. 539–553, Springer, 2000.

- [3] D. D. Morris and T. Kanade, "A unified factorization algorithm for points, line segments and planes with uncertainty models," in *Sixth International Conference on Computer Vision (IEEE Cat. No. 98CH36271)*, pp. 696–702, IEEE, 1998.
- [4] C. Bregler, A. Hertzmann, and H. Biermann, "Recovering non-rigid 3D shape from image streams," in *Computer Vision and Pattern Recognition, 2000. Proceedings. IEEE Conference on*, vol. 2, pp. 690–696, IEEE, 2000.
- [5] J. Xiao, J.-x. Chai, and T. Kanade, "A closed-form solution to non-rigid shape and motion recovery," in *European conference on computer vision*, pp. 573–587, Springer, 2004.
- [6] A. Bartoli, V. Gay-Bellile, U. Castellani, J. Peyras, S. Olsen, and P. Sayd, "Coarse-to-fine low-rank structure-from-motion," in *Computer Vision and Pattern Recognition, 2008. CVPR 2008. IEEE Conference on*, pp. 1–8, IEEE, 2008.
- [7] L. Torresani, A. Hertzmann, and C. Bregler, "Nonrigid structure-from-motion: Estimating shape and motion with hierarchical priors," *IEEE transactions on pattern analysis and machine intelligence*, vol. 30, no. 5, pp. 878–892, 2008.
- [8] I. Akhter, Y. Sheikh, S. Khan, and T. Kanade, "Nonrigid structure from motion in trajectory space," in *Advances in neural information processing systems*, pp. 41–48, 2009.
- [9] J. Valmadre and S. Lucey, "General trajectory prior for non-rigid reconstruction," in *Computer Vision and Pattern Recognition (CVPR), 2012 IEEE Conference on*, pp. 1394–1401, IEEE, 2012.
- [10] P. F. Gotardo and A. M. Martinez, "Kernel non-rigid structure from motion," in *2011 International Conference on Computer Vision*, pp. 802–809, IEEE, 2011.
- [11] P. F. Gotardo and A. M. Martinez, "Computing smooth time trajectories for camera and deformable shape in structure from motion with occlusion," *IEEE Transactions on Pattern Analysis and Machine Intelligence*, vol. 33, no. 10, pp. 2051–2065, 2011.
- [12] T. Simon, J. Valmadre, I. Matthews, and Y. Sheikh, "Separable spatiotemporal priors for convex reconstruction of time-varying 3D point clouds," in *European Conference on Computer Vision*, pp. 204–219, Springer, 2014.
- [13] A. Agudo and F. Moreno-Noguer, "Force-based representation for non-rigid shape and elastic model estimation," *IEEE transactions on pattern analysis and machine intelligence*, vol. 40, no. 9, pp. 2137–2150, 2018.
- [14] M. Lee, C.-H. Choi, and S. Oh, "A procrustean markov process for non-rigid structure recovery," in *Proceedings of the IEEE Conference on Computer Vision and Pattern Recognition*, pp. 1550–1557, 2014.
- [15] I. Akhter, Y. Sheikh, and S. Khan, "In defense of orthonormality constraints for nonrigid structure from motion," in *Computer Vision and Pattern Recognition, 2009. CVPR 2009. IEEE Conference on*, pp. 1534–1541, IEEE, 2009.
- [16] K. Fragkiadaki, M. Salas, P. Arbelaez, and J. Malik, "Grouping-based low-rank trajectory completion and 3D reconstruction," in *Advances in Neural Information Processing Systems*, pp. 55–63, 2014.
- [17] Y. Dai, H. Li, and M. He, "A simple prior-free method for non-rigid structure-from-motion factorization," *International Journal of Computer Vision*, vol. 107, no. 2, pp. 101–122, 2014.
- [18] Y. Zhu, D. Huang, F. De La Torre, and S. Lucey, "Complex non-rigid motion 3D reconstruction by union of subspaces," in *Proceedings of the IEEE Conference on Computer Vision and Pattern Recognition*, pp. 1542–1549, 2014.
- [19] S. Kumar, Y. Dai, and H. Li, "Spatio-temporal union of subspaces for multi-body non-rigid structure-from-motion," *Pattern Recognition*, vol. 71, pp. 428–443, 2017.
- [20] Y. Gu, F. Wang, Y. Chen, and X. Wang, "Monocular 3D reconstruction of multiple non-rigid objects by union of non-linear spatial-temporal subspaces," in *Proceedings of the 2nd International Conference on Vision, Image and Signal Processing*, p. 14, ACM, 2018.
- [21] A. Agudo and F. Moreno-Noguer, "DUST: Dual union of spatio-temporal subspaces for monocular multiple object 3D reconstruction,"
- [22] R. Cabral, F. De la Torre, J. P. Costeira, and A. Bernardino, "Unifying nuclear norm and bilinear factorization approaches for low-rank matrix decomposition," in *Proceedings of the IEEE International Conference on Computer Vision*, pp. 2488–2495, 2013.
- [23] C. Kong and S. Lucey, "Deep non-rigid structure from motion," in *Proceedings of the IEEE International Conference on Computer Vision*, pp. 1558–1567, 2019.
- [24] C. Wang, C. Kong, and S. Lucey, "Distill knowledge from NRSfM for weakly supervised 3D pose learning," in *Proceedings of the IEEE International Conference on Computer Vision*, pp. 743–752, 2019.
- [25] R. Hartley and A. Zisserman, *Multiple view geometry in computer vision*. Cambridge university press, 2003.
- [26] D. D. Morris, K. Kanatani, and T. Kanade, "Uncertainty modeling for optimal structure from motion," in *International Workshop on Vision Algorithms*, pp. 200–217, Springer, 1999.
- [27] T. Bailey, J. Nieto, J. Guivant, M. Stevens, and E. Nebot, "Consistency of the EKF-SLAM algorithm," in *2006 IEEE/RSJ International Conference on Intelligent Robots and Systems*, pp. 3562–3568, IEEE, 2006.
- [28] Y. Chen, J. Fan, C. Ma, and Y. Yan, "Inference and uncertainty quantification for noisy matrix completion," *arXiv preprint arXiv:1906.04159*, 2019.
- [29] R. Vidal and D. Abremske, "Nonrigid shape and motion from multiple perspective views," in *European conference on computer vision*, pp. 205–218, Springer, 2006.
- [30] S. Ma, D. Goldfarb, and L. Chen, "Fixed point and bregman iterative methods for matrix rank minimization," *Mathematical Programming*, vol. 128, no. 1-2, pp. 321–353, 2011.
- [31] Y. Chen, Y. Chi, J. Fan, C. Ma, and Y. Yan, "Noisy matrix completion: Understanding statistical guarantees for convex relaxation via nonconvex optimization," *arXiv preprint arXiv:1902.07698*, 2019.
- [32] "CMU graphics lab motion capture database." <http://mocap.cs.cmu.edu/>. Accessed: 2019-04-10.